Supplemental Figure 1

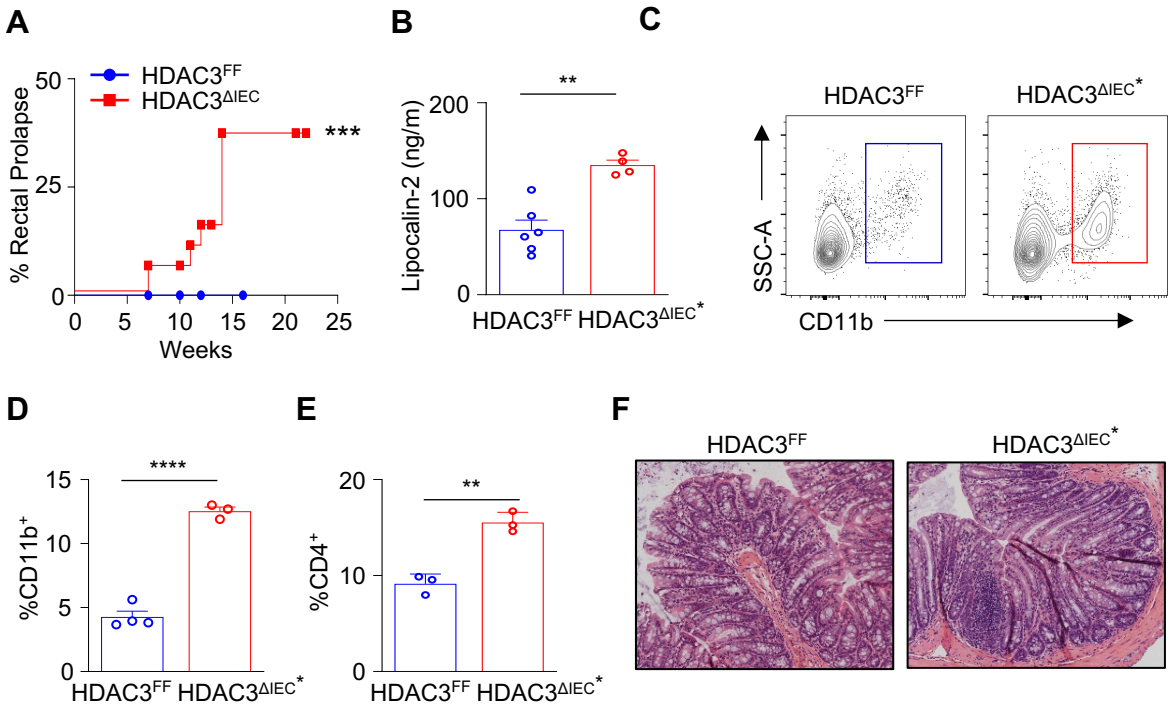

Supplemental Fig. 1. Loss of epithelial HDAC3 expression increases spontaneous intestinal inflammation. (**A**) Frequency of rectal prolapse in HDAC3^{FF} and HDAC3$^{\Delta IEC}$ mice. (**B**) Fecal concentrations of lipocalin-2. (**C, D**) Frequency of CD11b^{+} myeloid cells (Gated Live, CD45^{+}, CD3^{-}) and (**E**) frequency of intestinal CD4^{+} T cells (Gated Live, CD45^{+}) in the large intestine of HDAC3^{FF} and prolapse (*) HDAC3$^{\Delta IEC}$ mice. (**F**) H&E-stained colonic sections. Data represent at least three independent experiments, 3-6 mice per group. **p<0.01, ***p<0.001, ****p<0.0001.

Supplemental Figure 2

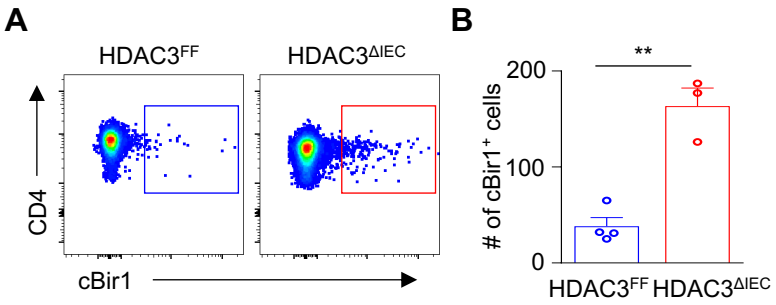

Supplemental Fig. 2. HDAC3 regulates commensal-specific T cells in the small intestine. (**A, B**) Number of cBir1+ CD4 T cells in small intestine of $HDAC3^{FF}$ and $HDAC3^{\Delta IEC}$. $cBir1^{+}$ tetramer cells are gated on live, $CD45^{+}$, lineage $(CD11b, B220, Ly6G, CD11c, CD8a)^{-}$, $CD4^{+}$. Data represent at least three independent experiments, 3-4 mice per group. **$p<0.01$.

Supplemental Figure 3

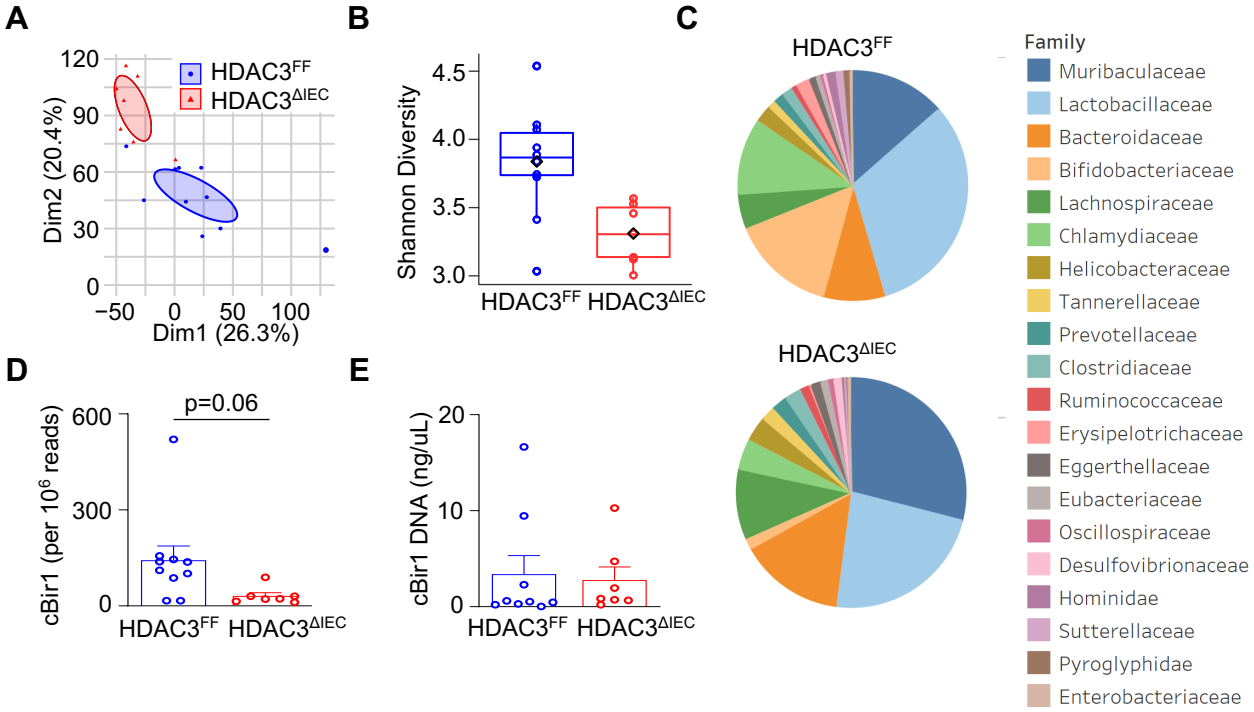

Supplemental Fig. 3. Intestinal microbiota composition in HDAC3^{FF} and HDAC3$^{\Delta IEC}$ mice. (**A**) PCA plot, (**B**) Shannon diversity, and (**C**) bacterial composition in HDAC3^{FF} and HDAC3$^{\Delta IEC}$ mice from metagenomic analyses of stool sample. (**D**) cBir1 counts per million reads and (**E**) cBir1 by qPCR in stool of HDAC3^{FF} and HDAC3$^{\Delta IEC}$ mice.

Supplemental Figure 4

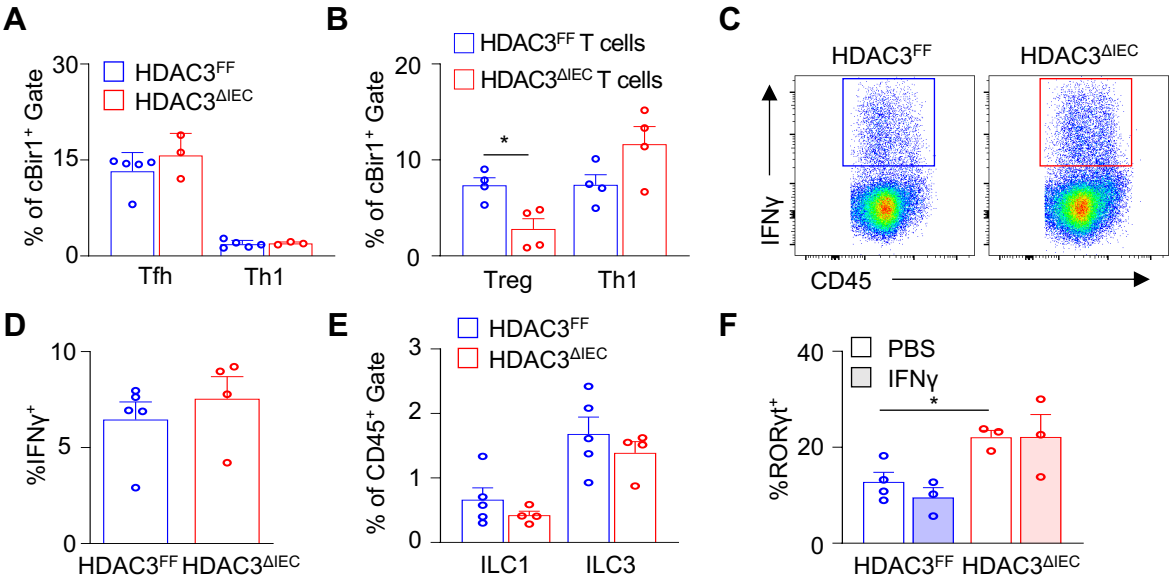

Supplemental Fig. 4. Intestinal immune responses in HDAC3$^{\Delta IEC}$ mice. (**A**) Frequency of Th subsets of cBir1^{+}CD4^{+} T cells from the large intestine of HDAC3^{FF} and HDAC3$^{\Delta IEC}$. (**B**) Frequency of Th subsets of cBir1^{+} commensal-specific T cells following transfer into Rag1$^{-/-}$ mice. cBir1^{+} tetramer cells are gated on live, CD45^{+}, lineage (CD11b, B220, Ly6G, CD11c, CD8a)$^{-}$, CD4^{+}. T follicular (Tfh) cells gated cBir1^{+}, FoxP3^{-}, CXCR5^{+}; Th1 cells gated cBir1^{+}, FoxP3^{-}, CXCR5^{-}, RORγt^{-}, Tbet^{+}. (**C, D**) Frequency of IFNγ^{+} CD45^{+} cells and (**E**) frequency of ILC1s and ILC3s in large intestine of HDAC3^{FF} and HDAC3$^{\Delta IEC}$ mice at steady state. (**F**) Frequency of RORγt^{+} cBir1^{+} cells in intestine of HDAC3^{FF} and HDAC3$^{\Delta IEC}$ mice treated with PBS or IFNγ. Data represent at least two independent experiments, 3-5 mice per group. *$p<0.05$.

Supplemental Figure 5

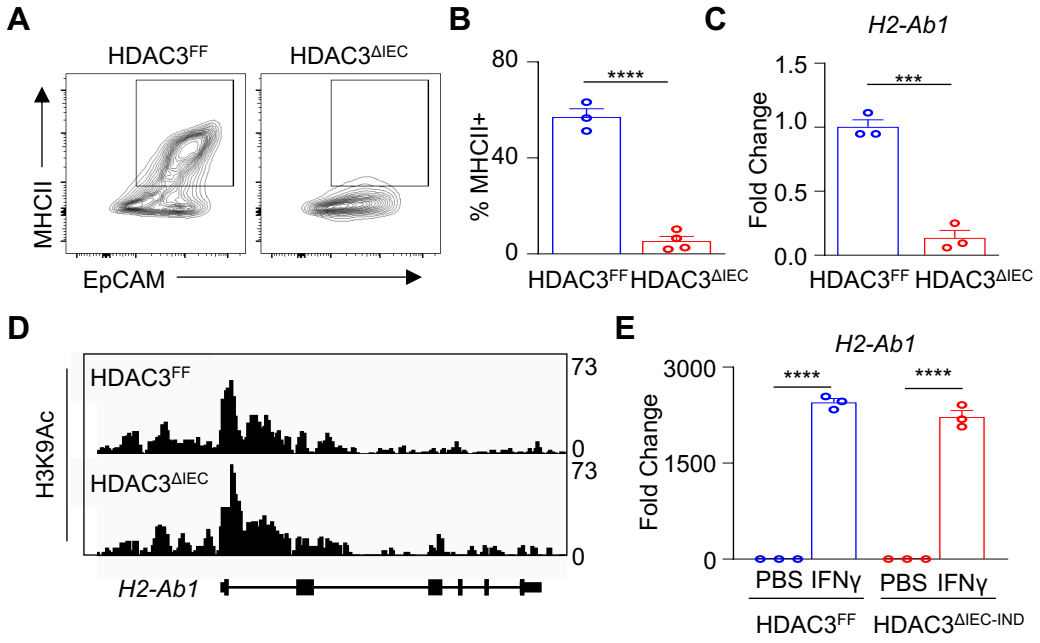

Supplemental Fig. 5. Histone acetylation and IFNγ induction of *H2-Ab1* are not significantly altered in IECs lacking HDAC3. (**A, B**) Frequency of MHCII^{+} IECs from small intestine of HDAC3^{FF} and HDAC3$^{\Delta IEC}$ mice. (**C**) H2-Ab1 mRNA expression in small intestinal IECs from of HDAC3^{FF} and HDAC3$^{\Delta IEC}$ mice. (**D**) ChIP-seq for H3K9Ac in primary IECs isolated from the large intestine. (**E**) H2-Ab1 mRNA expression in HDAC3^{FF} and HDAC3$^{\Delta IEC\text{-}IND}$ organoids treated with PBS or IFNγ. Data are representative of at least two independent experiments, 3-4 mice per group. ***$p<0.001$, ****$p<0.0001$.

Supplemental Figure 6

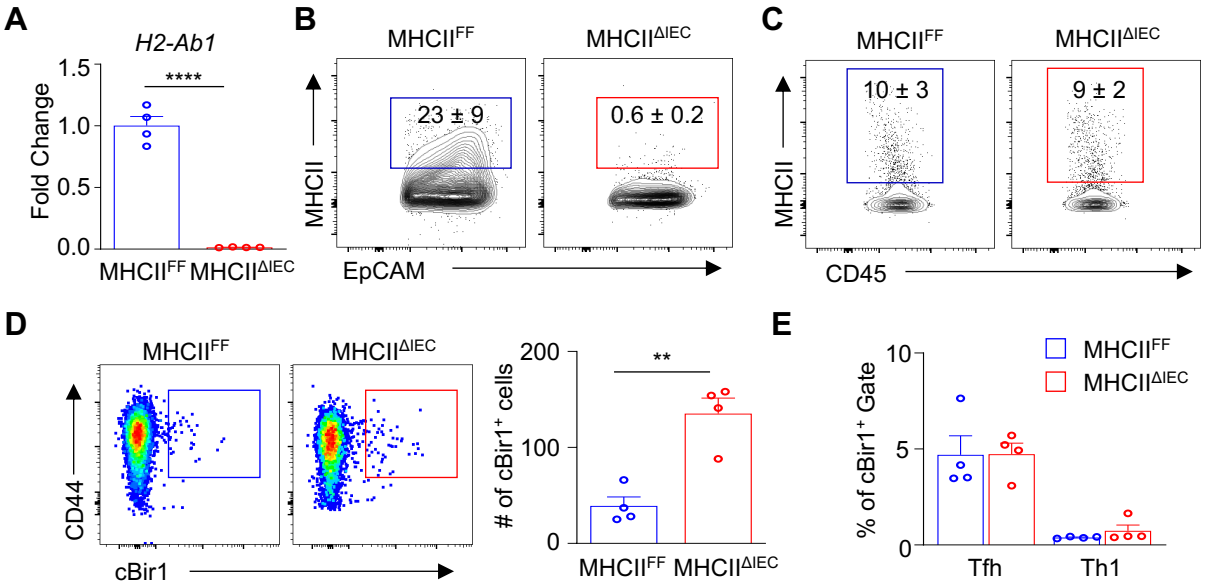

Supplemental Fig. 6. Confirmation of IEC-specific depletion of MHCII. (**A**) H2-Ab1 mRNA expression in IECs isolated from the large intestine of MHCII^{FF} and MHCII$^{\Delta IEC}$ mice. (**B**) Surface MHCII expression in EpCAM^{+}, CD45^{-} cells from MHCII^{FF} and MHCII$^{\Delta IEC}$ mice. (**C**) Surface MHCII expression in EpCAM^{-}, CD45^{+} cells from MHCII^{FF} and MHCII$^{\Delta IEC}$ mice. (**D**) Number of cBir1^{+} CD4^{+} T cells in small intestine of MHCII^{FF} and MHCII$^{\Delta IEC}$ mice. (**E**) Frequency of Th subsets of cBir1^{+}CD4^{+} T cells from colon of MHCII^{FF} and MHCII$^{\Delta IEC}$ mice. cBir1^{+} tetramer cells are gated on live, CD45^{+}, lineage (CD11b, B220, Ly6G, CD11c, CD8a)$^{-}$, CD4^{+}. T follicular (Tfh) cells gated cBir1^{+}, FoxP3^{-}, CXCR5^{+}; Th1 cells gated cBir1^{+}, FoxP3^{-}, CXCR5^{-}, RORγt^{-}, Tbet^{+}. Data represent at least three independent experiments, 3-4 mice per group. **$p<0.01$, ****$p<0.0001$

Supplemental Figure 7

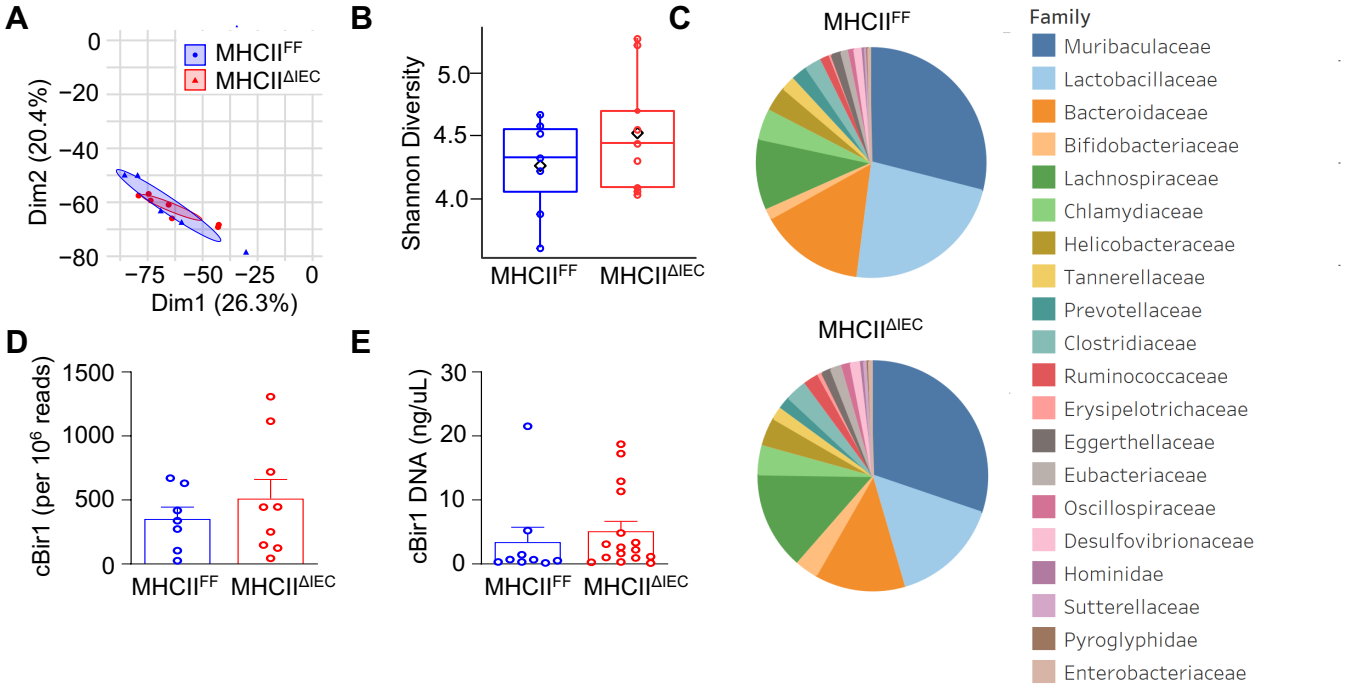

Supplemental Fig. 7. Intestinal microbiota composition in MHCII^{FF} and MHCII$^{\Delta IEC}$ mice. (**A**) PCA plot, (**B**) Shannon diversity, and (**C**) bacterial composition in MHCII^{FF} and MHCII$^{\Delta IEC}$ mice from metagenomic analyses of stool sample. (**D**) cBir1 counts per million reads and (**E**) cBir1 by qPCR in stool of in MHCII^{FF} and MHCII$^{\Delta IEC}$ mice.

Supplemental Figure 8

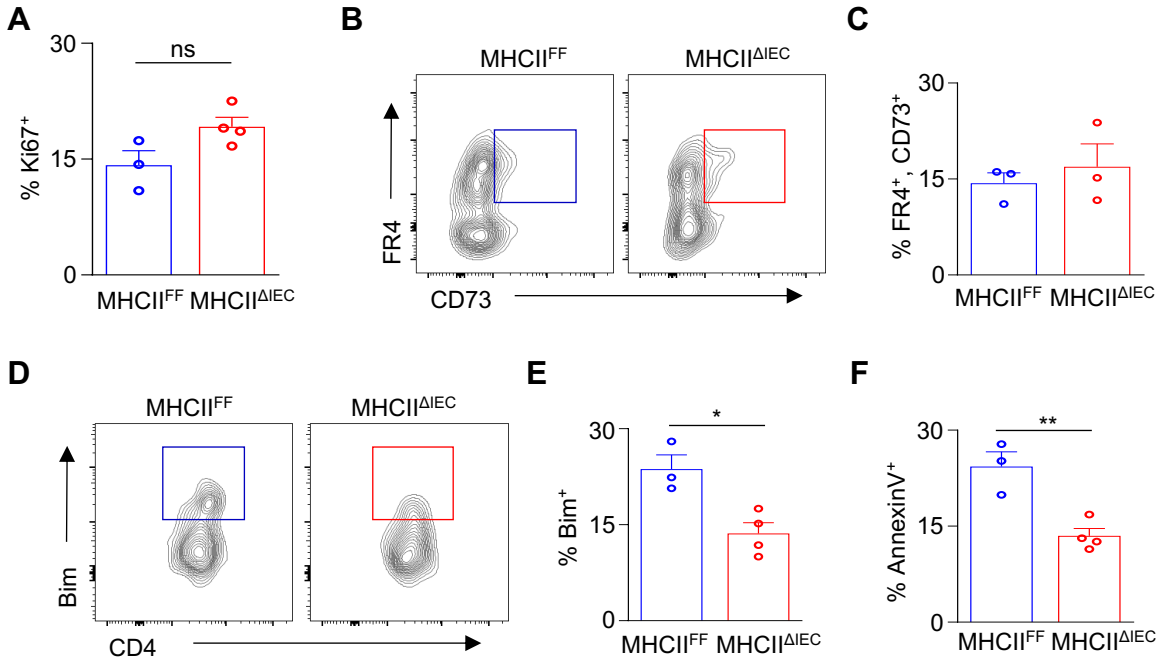

Supplemental Fig. 8. Commensal-specific CD4⁺ T cells from MHCII$^{\Delta IEC}$ mice exhibit reduced markers of apoptosis. (**A**) Frequency of Ki67⁺, (**B**, **C**) FR4⁺, CD73⁺, (**D**, **E**) Bim⁺ in cBir1⁺ CD4⁺ T cells from the large intestine of MHCII^{FF} and MHCII$^{\Delta IEC}$ mice. (**F**) Frequency of AnnexinV⁺ antigen experienced intestinal CD4⁺ T cells from the large intestine of MHCII^{FF} and MHCII$^{\Delta IEC}$ mice. Data represent at least two independent experiments, 3-4 mice per group. *$p<0.05$, **$p<0.01$, ns=not significant.

Supplemental Figure 9

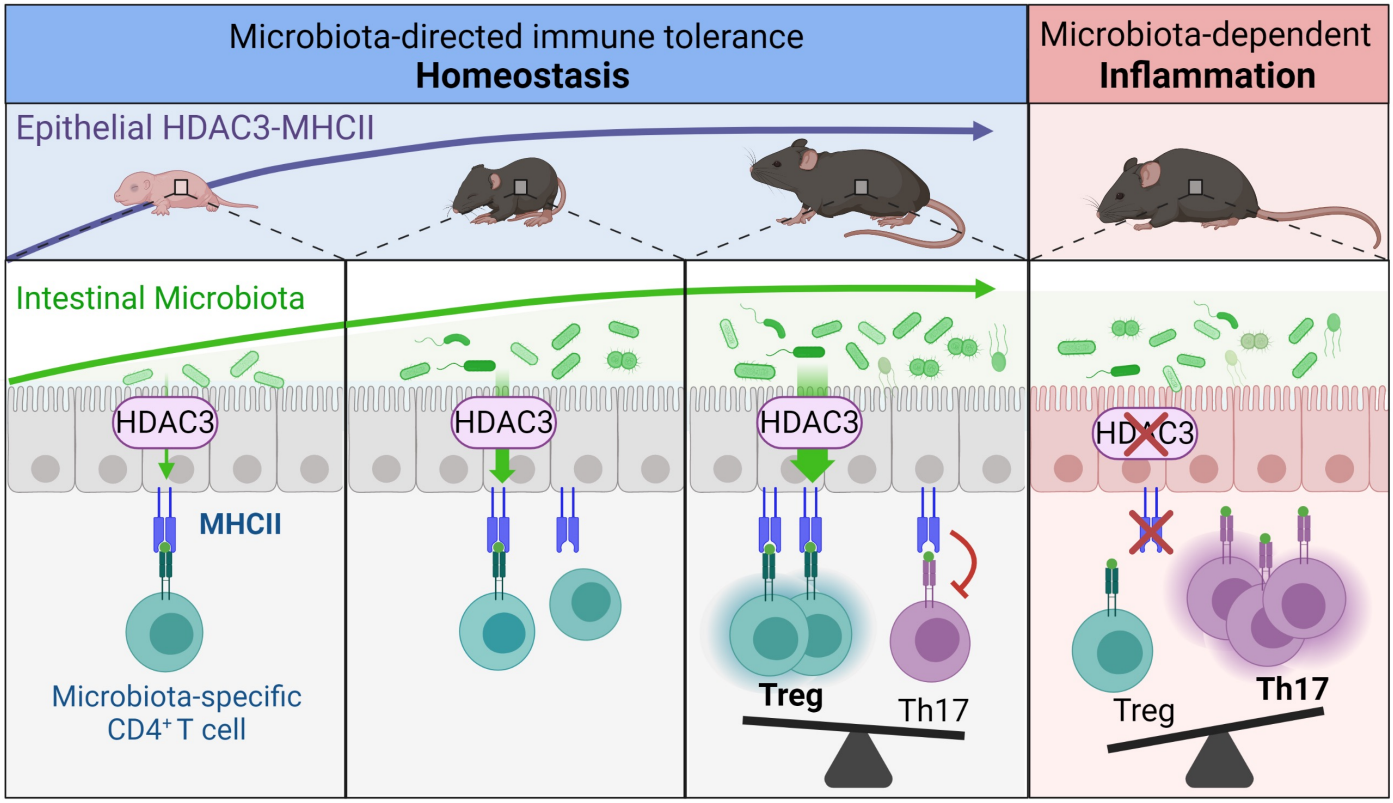

Supplemental Fig. 9. Intestinal epithelial MHC class II regulation by HDAC3 instructs microbiota-specific CD4⁺ T cells. HDAC3 regulation of epithelial MHCII is activated early and concurrently with microbiota colonization. This pathway is necessary to control local accumulation of T cells that respond to commensal microbes later in life. Loss of intestinal epithelial HDAC3 results in reduced commensal-specific Tregs and an increase in commensal-specific Th17 cells. Thus, microbiota drive tolerance in the intestine by inducing an epithelial mechanism that directs local CD4⁺ T cell subsets that recognize commensal antigens and decrease susceptibility to microbiota-sensitive inflammation. Created with Biorender.com.